Original Article

Institution of MECHANICAL ENGINEERS

Journal of RAIL AND RAPID TRANSIT

Proc IMechE Part F:
J Rail and Rapid Transit
0(0) 1–16

DOI: 10.1177/0954409716642485
pif.sagepub.com

SAGE

A mechanistic model of lateral rail head deflection based on fastening system parameters

Zhe Chen and Bassem Andrawes

Abstract

This paper presents a mechanistic model of the rail head lateral deflection with the aim of quantifying the distribution of the lateral wheel load in a concrete sleeper rail track. The model is developed based on observations of the field experimentation and the results of a three-dimensional validated finite element model. The input parameters of the model are primarily based on the design of the fastening system and the track structure. In the developed model, the rail head lateral deflection is divided into two components which are computed separately: rail base lateral deflection and rail head rotational deflection. The model considers the possible gap between the field-side shoulder and insulator, and assumes Coulomb Law of friction for the rail base interfaces. Based on an experimental design approach, the prediction of the mechanistic model is compared with that of finite element model as well as with field data.

Keywords

Mechanistic design, rail deflection, track gage, fastening system, finite element analysis

Date received: 7 March 2015; accepted: 6 August 2015

Introduction

In the recent decades, large number of the concrete crossties have been installed on North America railroad tracks. Compared to the crossties made of other materials (wood, polymeric composite, etc.), the concrete sleeper is more suitable for severe loading scenarios, including high-speed passenger rail and heavy axle load freight traffic for higher material strength and longer lifespan.[1] To securely transfer the wheel loads from the wheels to the crossties and maintain proper track geometry, a set of fastening system is installed at each rail seat. Some evaluative tests are specified in the American Railway Engineering and Maintenance-of-way Association (AREMA) Manual for Railway Engineering to ensure the quality and performance of the fastening system on the concrete sleeper.[2] However, the lateral wheel load path through the concrete crossties and fastening systems, as well as the effect of the fastening system design on the track performance is not clearly defined. Considering the ever-increasing axle load of freight trains and the development of higher speed passenger rail, a mechanistic design methodology is needed so that the design of the fastening system can be related to the track performance under a certain loading scenario. To develop such a mechanistic design methodology, it is critical to quantify the path of the lateral wheel load through the concrete crossties and the fastening systems.

One of the most critical functionalities of a fastening system is to maintain uniform track geometry. In the Track and Rail and Infrastructure Integrity Compliance Manual published by Federal Railroad Administration (FRA), the allowable deviation of rail head from uniform geometry is defined for different track classes.[3] "Alinement" is defined as the line uniformity in horizontal plan of each rail, and "gage" is defined as the distance between the two rails measured 15.9 mm (0.625 in) below the top surface of the rail. Both the alinement and the gage of a track section are related to the performance of the fastening system under lateral wheel load. While some pass/fail evaluative tests are defined in the AREMA Manual to ensure the quality of the fastening system, limited guideline is provided for railroad engineers to design or verify a fastening system toward the requirement of a certain track class.

Department of Civil and Environmental Engineering, University of Illinois at Urbana-Champaign, Urbana, USA

Corresponding author:
Bassem Andrawes, Department of Civil and Environmental Engineering, University of Illinois at Urbana-Champaign, Urbana, IL 61801, USA.
Email: andrawes@illinois.edu

The research necessity about the design of fastening system is also confirmed by an international survey conducted by the Rail Transportation and Engineering Center at the University of Illinois at Urbana-Champaign. The survey focused on the railway industry's state of practice regarding the concrete crossties and fastening system design, performance and research needs, and was sent to railroad infrastructure manufacturers and major railroad companies both in the North America and other parts of the world.[4] Based on the results of the survey, the most prevalent failure causes which result in the deficiency of concrete sleeper and fastening system were highlighted. While the international response and domestic responses (North America) were quite different, "fastening system damage" and "improper component design" are frequently reported to be associated with the operating environment of both international and domestic respondents. Based on the results of the international survey, it can be observed that the design and damage of the fastening system has become an important concern for railroad infrastructure and should be further investigated. In this study, a mechanistic model of basic structural components is proposed to estimate the rail head lateral deflection relative to the concrete sleeper based on the design of the fastening system. The mechanistic model is derived based on the field-validated finite element (FE) model of one design of the concrete sleeper and fastening system; however, it is generalized and can be applied to fastening systems of different designs. The model is then validated numerically and using field data to ensure its capability to capture the behaviors of different fastening systems within the design space.

Background on mechanistic models

On North America railroad tracks, fastening systems of different designs are installed, and each unique design of the fastening system includes different components. Generally, most fastening systems include rail clips, insulators, rail pads, and fixtures casted in the concrete. Figure 1 shows an example of fastening system installed on North America tracks. The system includes cast iron shoulders, nylon insulators, polymer rail pads, and steel rail clips. The shoulders are casted into concrete to provide fixture for other fastening system components. The clips are inserted into the shoulders and predeformed to restrain possible rail deflection. The nylon insulators are placed between the rail clips and the rail to ensure electric isolation between the two rails. The rail pad is installed between the rail and the concrete crossties to attenuate the dynamic wheel load and reduce rail seat abrasion.

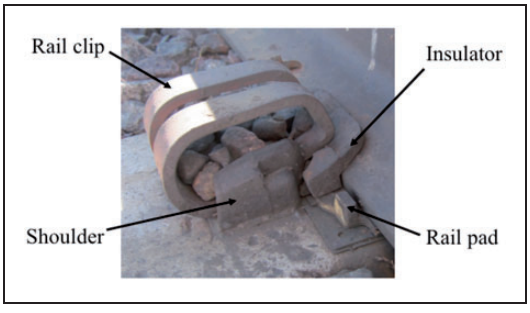

Figure 1. Example design of fastening system on North America railroads.

To understand the existing knowledge on the performance and design of the track structure, previous experimental and analytical studies on the rail deflection under vertical and lateral wheel loadings are summarized. Researchers have looked into the deflection of the rail under different wheel loading scenarios as it is related to the deviation of uniform track geometry and some severe track failure modes including rail rollover. The early experimental and analytical studies were summarized by Zarembski.[5] Marquis et al.[6] conducted closed-form analysis to examine combinations of wheel/rail loads and contact conditions that result in high rail seat pressure or rail rollover. The analysis assumed that the vertical and lateral wheel loads applied are solely balanced by the loaded rail seat reaction. However, as the wheel loads distribute over multiple rail seats on actual track, the result of the study could overestimate the rotation of the rail. Similar assumptions were made in some other studies on rail rollover.[7,8]

To theoretically understand and simplify the track structure, mechanistic models are often proposed based on finite element simulation or field observation. A mechanistic model describes a system based on the fundamental physical laws that it obeys and looks into the functions of the system components. One example of the mechanistic model is the theoretical model that Talbot proposed to describe the behavior of track structure under vertical wheel load.[9] In the theoretical model, the track structure is simulated as a continuous beam on elastic foundation. The characteristics (material property and moment of area) of the continuous beam are determined by that of the rail, and the stiffness of the elastic foundation, which represents track substructure, is named "track foundation modulus" and determined based on field experimentation. Winkler foundation is considered in this model and "track foundation modulus" was defined as "the pressure per unit length of each rail necessary to depress the track one unit." This model serves as the basis for a number of improved models, and it is still used in some design standards for the calculation of rail stress and deflection.

Field experimentation in the 1970s mainly focused on the gage widening effect under wheel loads, and the translation and rotation of the rails were observed in the process.[10] Based on the observations in the experimentations, some preliminary models were proposed

to describe the lateral behavior of the track. Sato[11] proposed a model of three springs to simulate the behavior of the track structure under lateral wheel load: a spring to represent the lateral displacement of sleeper relative to the ballast, a spring to represent the translational displacement of the rail head relative to the sleeper, and a spring to represent the rotational displacement of the rail head relative to the sleeper. The total displacement of the three springs sum up to the absolute lateral displacement of the rail head.

Timoshenko and Langer[12] presented a mechanistic model to describe the response of railroad track under lateral wheel load, in which the rail is assumed to be continuously supported with continuous springs resisting its translation and rotation. The mechanistic model is easy to use; however, some of the spring constants are not clearly related to the design of the track structure and can only be obtained through field experimentation. Arbabi-Kanjoori[13] used the variational method to determine the stiffness matrix of the continuous track structure under vertical, lateral, and longitudinal wheel load. The model also considered some generalized springs that could only be determined experimentally. Turek[14] proposed an analytical model that simulates the nonlinear static behavior of the track superstructure. The model includes a track section of 26 crossties and considers the translation and rotation of the rail under a combination of vertical and lateral wheel load. However, the nonlinear stiffness included in the model could only be determined through experimentations. In general, the existing analytical and experimental studies on rail deflection under the lateral wheel load provide some insight on the characteristic of the track structure; however, they are either oversimplified or heavily dependent on field measurement.

Development of the mechanistic model of the rail head lateral deflection

In the mechanistic model proposed in this study, under lateral wheel load the rail is assumed to be a continuous beam on discrete supports, and the supports are placed at the positions of the rail seats. Based on the tests and studies presented by Timoshenko and Langer,[12] the lateral bending and torsion of the rail are local behaviors, and the superposition of two lateral wheel loads is insignificant considering the wheel spacing. Therefore, a single lateral wheel load is considered in the mechanistic model. As this study focuses on the rail lateral deflection relative to the sleeper, symmetric loading scenario is assumed where identical vertical and lateral wheel loads (gauge-splitting load) are applied over the two rails, and half of the track section is considered. In addition, in field experimentation and FE analysis it is also observed that the lateral wheel load is mainly distributed among the three nearest rail seats,[15] and therefore three discrete supports are included in the model.

Previously a FE model of prestressed concrete sleeper and fastening system was built in ABAQUS[16] and validated with laboratory and field experimentation[17] (see Figure 2). It is proven during the model validation that the FE model is able to capture some critical mechanisms of the track structure including the rotation of the rail, the response of the fastening system, the distribution of the wheel loads, and the flexure of the concrete sleeper. The validated FE model is used in this study to derive several of the parameters assumed for the mechanistic model.

In the model, the rail head lateral deflection under lateral wheel load is divided into two components: the rail base lateral deflection (RBLD) and the rail head rotational deflection (RHRD) relative to the rail base,

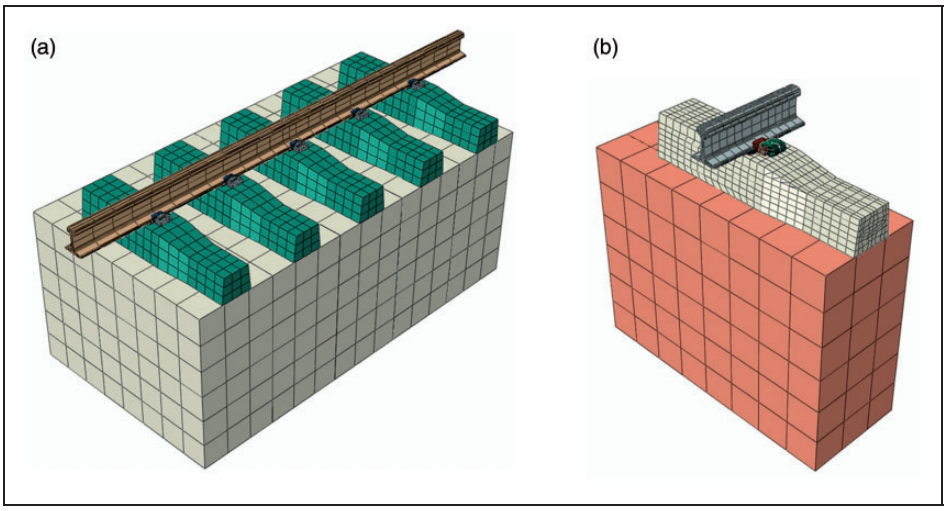

Figure 2. Field-validated (a) global finite element model and (b) detailed finite element model.

as shown in Figure 3. The mechanistic model assumes the superposition of the rail lateral bending and torsion under eccentric lateral wheel load. The RBLD is associated with the lateral bending of the rail, and the RHRD is associated with the torsion of the rail. Two models are developed to determine the two components of rail head lateral deflection as explained in the following discussion.

Mechanistic model for RBLD

The framework for the RBLD model is shown in Figure 4(a). k_1 is the lateral stiffness of the loaded rail seat, and k_2 is the lateral stiffness of the adjacent rail seat. The lateral wheel load is applied at one rail seat and distributes among the three nearest rail seats. At each rail seat, as shown in Figure 4(b) the lateral rail seat load is resisted by the shoulder bearing force and the rail pad frictional force. Considering the coefficient of friction (COF) at the clip–insulator interface and the magnitude of clamping force, the friction at the interface has minor contribution to the lateral load path within the fastening system. This is also proven in preliminary parametric studies. In other words

$$L = R_1 + 2R_2 \tag{1}$$

$$R_1 = F_P + F_{SI} \tag{2}$$

where L is the applied lateral wheel load, R_1 is the rail seat lateral load at the loaded rail seat, and R_2 is the

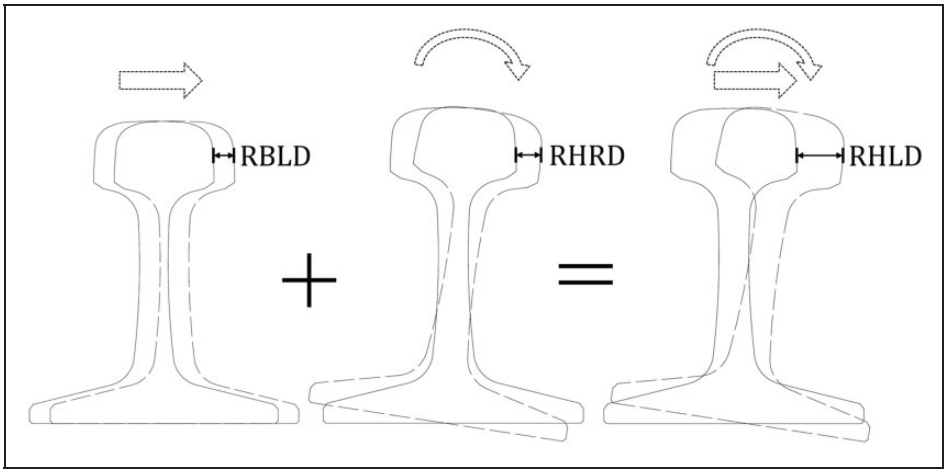

Figure 3. Deflection of the rail under lateral wheel load.

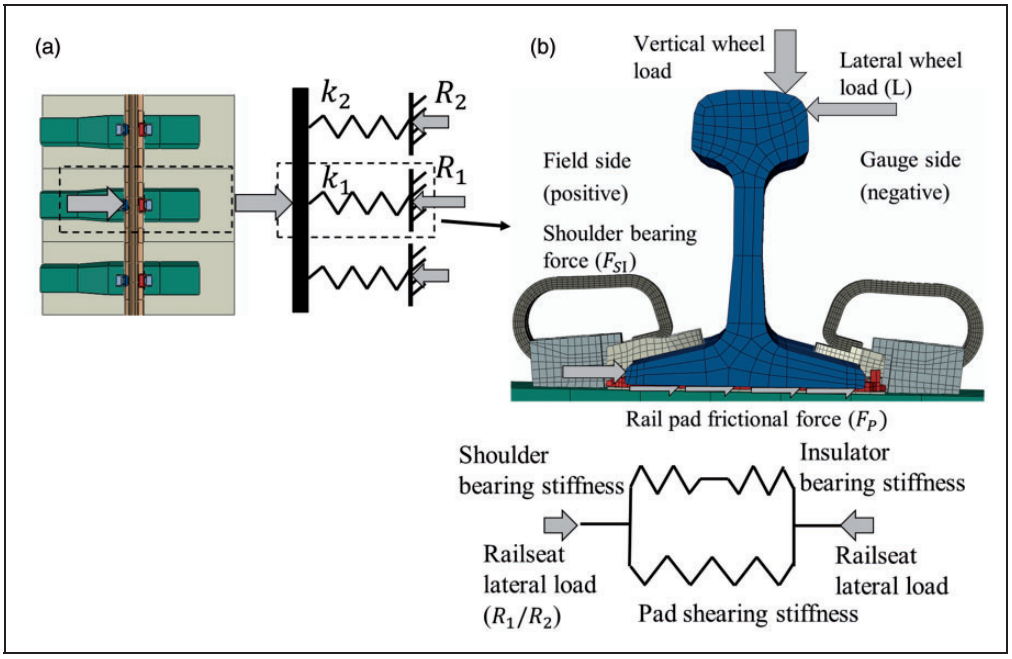

Figure 4. Mechanistic model of the track structure under lateral wheel load: (a) at multiple rail seats and (b) within one rail seat.

rail seat lateral load at the adjacent rail seat. F_P is the rail pad frictional force, and F_{SI} is the shoulder bearing force.

The Coulomb law is assumed for at the interfaces between rail base, rail pad, and concrete. Hence, no relative sliding is allowed at these interfaces until the frictional force exceeds the threshold. Identical COF is assumed at the interfaces for similar frictional properties. It is also observed in preliminary parametric studies based on the validated FE model that the COF at the two interfaces has identical effect on the lateral load path within the fastening system. The lateral resistance of the fastening system at a rail seat can be modeled using a series of springs that represent the lateral stiffness of the fastening system components. To determine the lateral resistance of the fastening system, the loading scenario and the lateral stiffness of all fastening system components should be determined.

Insulator

Under lateral wheel load, the lower part of the field-side insulator is in compression between the shoulder and the rail base, as shown in Figure 5. Based on the geometry and material property of the insulator, the component stiffness can be determined as

$$K_{In} = \frac{E_{In} A_{In}}{d_{In}} \tag{3}$$

where E_{In} is the elastic modulus of insulator, d_{In} is the component thickness in compression, and A_{In} is the contact area between the rail base and the insulator.

Shoulder

The load scenario of the shoulder is more complicated as the shoulder inserts are embedded into concrete. As shown in Figure 5(b), in the FE model interaction is defined between the bottom of shoulder head and the concrete, and boundary condition is defined at the end of shoulder inserts. The FE model was validated with the field measurement, and good agreement between the experimental and numerical results indicated that the boundary condition and interaction defined in the FE model is able to capture the behavior of the shoulder in the field condition.[15] Considering the modeling technique in the FE model, the mechanistic model of the shoulder is defined as shown in Figure 6(c). Under the shoulder bearing force, the shoulder is assumed to be a cantilever beam. The length of the cantilever beam l_{SH} is the same as that of the shoulder insert. A rotational spring is attached to the top end of the cantilever beam to account for the effect of shoulder–concrete interaction, and a rigid portion that rotates with the end of the cantilever beam is added to account for the rotation of the shoulder head. Δ_I and θ_I are the deflection and rotation at the loaded end (shoulder insert top), respectively.

The stiffness of the rotational spring is calibrated based on the shoulder in the validated FE model. Due to the interaction between the shoulder and the concrete, the lateral stiffness of the shoulder is between that of a typical cantilever beam and a cantilever beam with rotational restraint at the loaded end. Figure 7 shows the force–displacement relationship of the shoulder inserts observed in the FE model under the same loading scenario and track condition as in the field experimentation.[15] The comparison is under a vertical wheel load of 178 kN (40 kips) and a lateral wheel load of 98 kN (20 kips), and the design of the fastening system is given in previous publication.[17] During the linear stage, and after a process of trial and error it was found that the stiffness of the shoulder insert can be closely described as

$$k_{insert} = \frac{F_{SI}}{\Delta_I} = \frac{5 E_{SH} I_{SH}}{l_{SH}^3} \tag{4}$$

where E_{SH} is the elastic modulus of the shoulder, I_{SH} is the area moment of inertia of the shoulder inserts, and l_{SH} is the length of the shoulder insert. k_{insert} can be considered as the effective stiffness of the cantilever

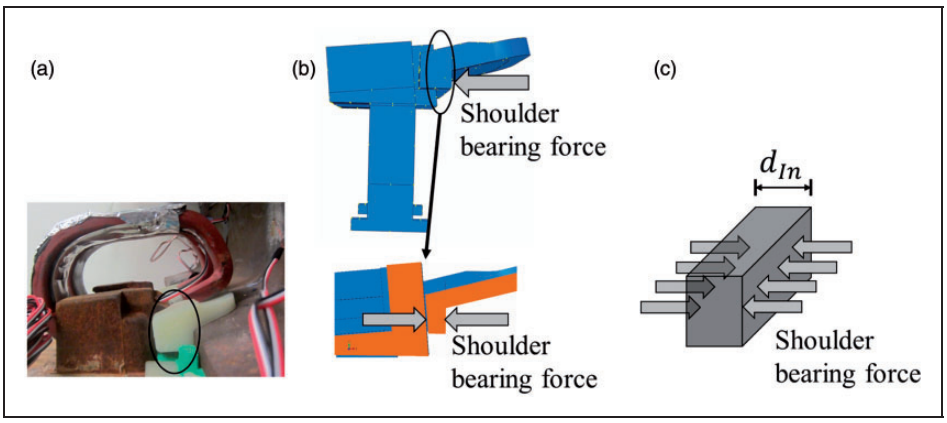

Figure 5. (a) Insulator in the fastening system, (b) loading scenario of the insulator, and (c) mechanistic model of insulator.

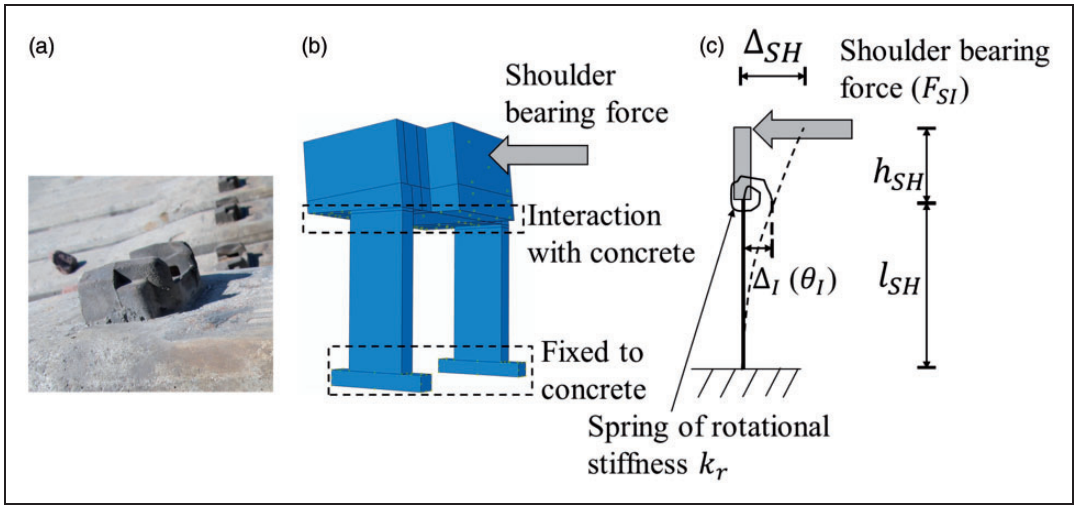

Figure 6. (a) Shoulder in the fastening system, (b) loading scenario of the shoulder in the validated FE model, and (c) mechanistic model of the shoulder.

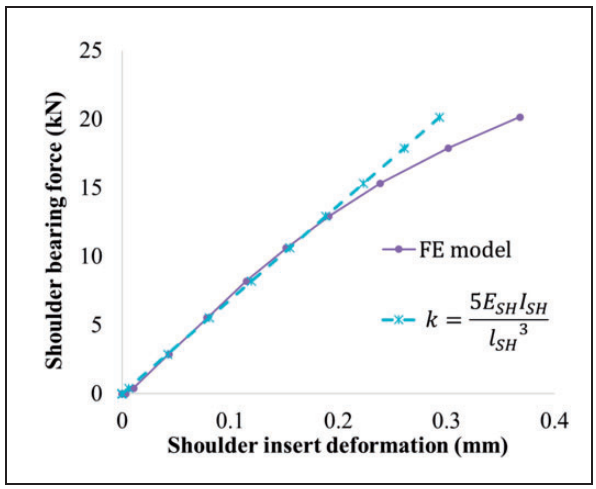

Figure 7. Example behavior of shoulder insert based on the FE model.

connected to a rotational spring with unknown stiffness k_r (see Figure 6). Based on equation (4) and the stiffness matrix of a cantilever beam, k_r can be determined as

$$k_r = \frac{8E_{SH}I_{SH}}{7l_{SH}} \tag{5}$$

In this mechanistic model, k_r is estimated based on the performance of one concrete crosstie and fastening system design, and it could be correspondingly estimated in different track system.

Based on k_r, the effective stiffness of the shoulder under shoulder bearing force can be determined as

$$K_{SH} = \frac{F_{SI}}{\Delta_{SH}} = \frac{F_{SI}}{\Delta_I + \Delta_r} = \frac{F_{SI}}{\frac{F_{SI}}{k_{insert}} + \theta_I h_{SH}} \tag{6}$$

where Δ_{SH} is the deflection of the shoulder, and Δ_r and h_{SH} are the rotational deflection and the height of the shoulder head, respectively (see Figure 6). As the insulator and the shoulder could be understood as two springs in series under lateral wheel load, the resultant lateral stiffness of the insulator and the shoulder is

$$K_{SI} = \frac{K_{In}K_{SH}}{K_{In} + K_{SH}} \tag{7}$$

where K_{In} and K_{SH} are component lateral stiffness of the insulator and the shoulder, respectively.

Rail pad

At a rail seat, part of the lateral rail seat load is resisted by the rail pad frictional force. Between the rail base and the concrete the rail pad is in shear, and the shear deflection of the rail pad at the field side equals to the RBLD before any relative sliding at the rail base interfaces. The shear stiffness of the rail pad can be determined as

$$K_P = \frac{0.5A_{RP}G_P}{d_P} \tag{8}$$

where A_{RP} is the nominal contact area between the rail base and the rail pad, G_P is the shear modulus of the rail pad, and d_P is the thickness of the rail pad (see Figure 8). Due to the rotation of the rail base, the rail pad is not in uniform shear, and only part of the nominal contact area is effective, as indicated by the rail pad contact pressure distribution obtained from the FE analysis (see Figure 8(b)). As a result half of the nominal contact area was assumed to be effectively in shear.

Based on the manufacturer design of the fastening system, there is a gap of about 0.127 mm (0.005 in)

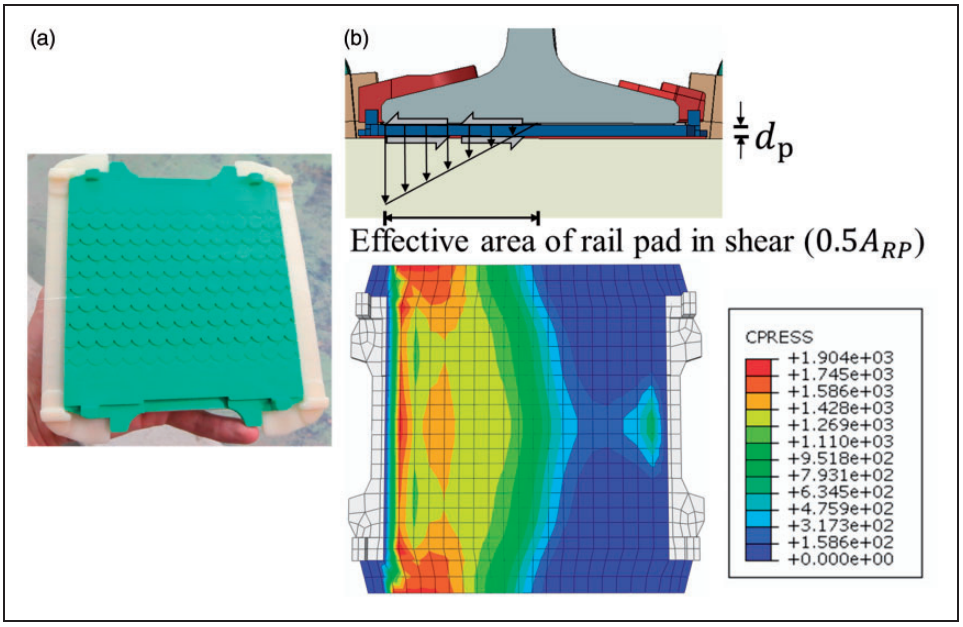

Figure 8. (a) Rail pad in the fastening system and (b) mechanistic model of rail pad in shear.

between field-side insulator and the shoulder, which could be closed under lateral wheel load. Before the shoulder–insulator gap is closed, all the lateral rail seat load is resisted by the rail pad frictional force. After the RBLD of a rail seat exceeds the gap size $\boldsymbol{\delta}$, the shoulder–insulator gap is closed and part of the lateral rail seat load is resisted by the shoulder bearing force. Considering the Coulomb law assumed for the rail seat interfaces, a fastening system could be under four different conditions as the shoulder–insulator gap could be open or closed, and the rail seat interfaces could be sticking or sliding. To correctly estimate the lateral stiffness of the rail seats, the condition of the fastening system needs to be determined based on the wheel loading scenario and the design of the fastening system. To simplify the mechanistic model, it is assumed that rail seat interfaces at the adjacent rail seats have no relative sliding and the shoulder–insulator gap at the adjacent rail seats is closed at the same time as the loaded rail seat. It is reasonable to assume sticking interfaces at adjacent rail seats as the sum of the clamping force and the rail seat vertical load at adjacent rail seats are usually sufficient to resist the relative sliding of the interfaces. In addition, as the rail's moment of inertia about vertical cross sectional axis I_R is relatively small and most of the lateral wheel load is resisted by the loaded rail seat, it could be proven that the second assumption about shoulder–insulator gap has minor effect on the calculation of the RBLD.

Figure 9 shows all four possible conditions of the fastening system. As in Figure 4, three rail seats are considered in the mechanistic model, and two springs are placed at each rail seat to represent the contribution of rail pad (K_P), and the combination of shoulder and insulator (K_{SI}), as discussed previously. The spring indicating the shoulder–insulator stiffness is marked with dash line when the shoulder–insulator gap is still open and is marked with solid line when the gap is closed. Under negligible lateral wheel load, the rail seat interfaces will be sticking and the shoulder–insulator gap will be open (Figure 9(a)). If the vertical wheel load maintains at the same magnitude and the lateral wheel load continues increasing, eventually the rail seat will slide on the rail pad, and the shoulder–insulator gap will be closed (Figure 9(d)). In Figure 9, F_{PS} is the maximum rail pad frictional force defined by the normal load on the rail pad and the COF of the interfaces.

Between the two extreme conditions, there are two alternative conditions based on the design of the fastening system. Under increasing lateral wheel load, if the shoulder–insulator gap is closed before the rail base starts to slide on the rail pad, the condition is described in Figure 9(b) (gap closed, sticking). Otherwise the rail base starts to slide on the rail pad before the shoulder–insulator gap is closed, and the condition is described in Figure 9(c) (gap open, sliding). The condition described in Figure 9(b) usually exists in fastening system with high COF and a soft rail pad, while the condition described in Figure 9(c) usually exists in fastening system with low COF and a stiff rail pad.

Figure 10 shows the procedure to determine the condition of the fastening system. First, model information on the design of the fastening system and the track is introduced to calculate the component stiffness under lateral wheel load. In the mechanistic model the distribution of vertical wheel load is assumed based on the recommendation in AREMA Manual, where the wheel load distribution on

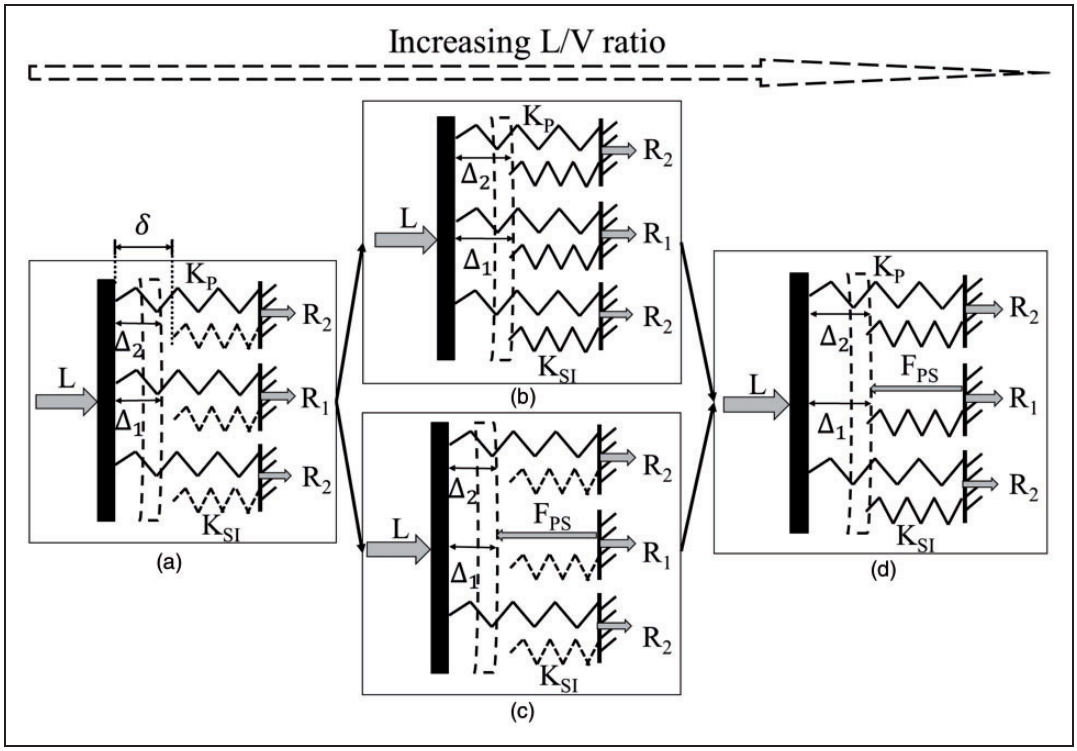

Figure 9. Different conditions of the fastening system under lateral wheel load including (a) gap open, sticking; (b) gap closed, sticking; (c) gap open, sliding; and (d) gap closed, sliding.

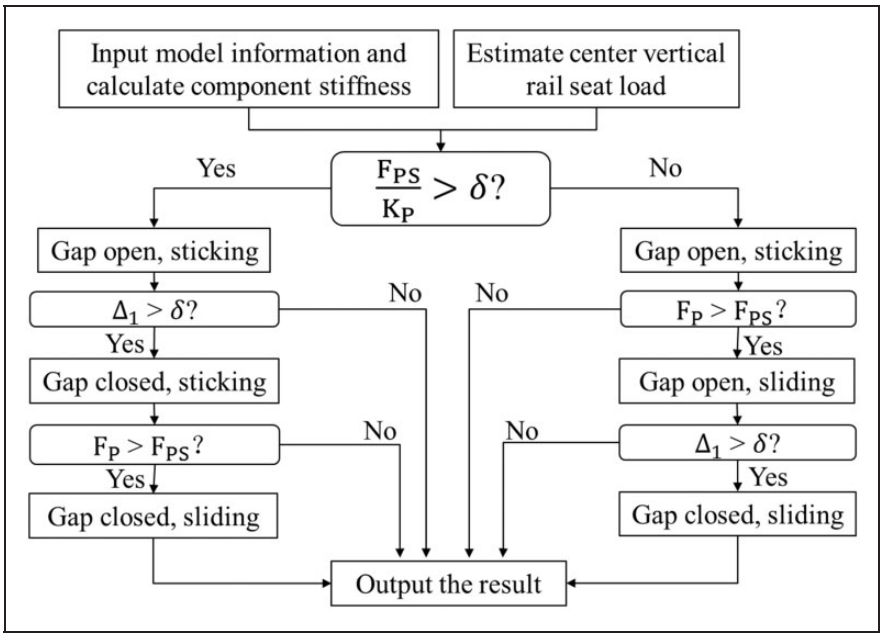

Figure 10. Procedure to determine the condition of the fastening system.

concrete sleeper track is determined as a function of sleeper spacing.[2] The normal load on the rail pad is determined as the sum of vertical rail seat load and the clamping force. Based on size of the shoulder–insulator gap $\boldsymbol{\delta}$ and the material property of the rail pad, the lateral rail seat load needed to close the gap can be determined and compared with the maximum rail pad frictional force F_{PS} to determine which of the two alternative conditions is representative of the fastening system.

After determining the possible conditions of a fastening system design, the result of calculation is checked against multiple criteria to ensure the correct rail seat lateral stiffness k_1/k_2 is used. Considering the rail as a beam in lateral flexure, based on the Euler–Bernoulli bending theory, the relationship between

the RBLD at the loaded rail seat and adjacent rail seat (Δ_1 (or RBLD) and Δ_2) can be determined as

$$\Delta_1(or\ RBLD) - \Delta_2 = \frac{(2R_2)(2sp)^3}{48E_RI_R} \quad (9)$$

where sp is the sleeper spacing, E_R is the elastic modulus of the rail, and I_R is the rail's moment of inertia about vertical cross sectional axis.

Table 1 shows the relationship between lateral rail seat stiffness k_1/k_2 and the RBLD Δ_1/Δ_2 based on different conditions of the fastening systems. Combining equations (1) and (9) and Table 1, under different conditions the lateral rail seat load R_1/R_2 and RBLD Δ_1/Δ_2 could be determined. The condition is slightly different when the shoulder–insulator gap is open and the rail base is sliding on the rail pad. In this case, the lateral load at the loaded rail seat is completely resisted by the rail pad frictional force at the maximum magnitude, and therefore

$$R_1 = F_{PS} \quad (10)$$

Table 1. Determination of rail seat lateral stiffness and rail base lateral deflection under different conditions.

Fastening system conditions	k_1	k_2	Δ_1	Δ_2
Gap open, sticking	K_P	K_P	$\frac{R_1}{k_1}$	$\frac{R_2}{k_2}$
Gap closed, sticking	$K_P + K_{SI}$	$K_P + K_{SI}$	$\frac{R_1+\delta K_{SI}}{k_1}$	$\frac{R_2+\delta K_{SI}}{k_2}$
Gap open, sliding	N/A	K_P	N/A	$\frac{R_2}{k_2}$
Gap closed, sliding	K_{SI}	$K_P + K_{SI}$	$\frac{R_1-F_{PS}}{k_1} + \delta$	$\frac{R_2+\delta K_{SI}}{k_2}$

which could be combined with equations (1) and (9) to determine Δ_1. The model initially assumes the shoulder–insulator gap is open and the rail seat interfaces are sticking. Afterward the calculated rail pad frictional force F_P and RBLD Δ_1 at the loaded rail seat are compared with the maximum frictional force F_{PS} and the size of the gap $\boldsymbol{\delta}$ to validate the assumption and determine the condition of the fastening system.

Mechanistic model for RHRD

As both the vertical and lateral wheel load and the rail seat reactions are not applied through the shear center of the rail, the rail rotates about the longitudinal axis and results in a difference between the rail head lateral deflection and the RBLD. To estimate the RHRD relative to the rail base, a mechanistic model is built as shown in Figure 11. In the validated FE model,[17] it is observed that the rail mainly rotates between the two adjacent rail seats, which agrees with the analysis of Timoshenko and Langer that the rotation and lateral bending of the rail are localized behavior.[12] As a result a beam with a length of twice the sleeper spacing is used to represent the rail in torsion.

To estimate the RHRD, the resultant torque due to the wheel loads and the rail seat reactions at each rail seat should be determined. The loading scenarios of the loaded and adjacent rail seats are shown in Figure 11. At all rail seats, the lateral rail seat load is resisted by the shoulder bearing force and the rail pad frictional force, which are both applied close to height of the rail base. Two clamping forces are applied symmetrically on the field side and the

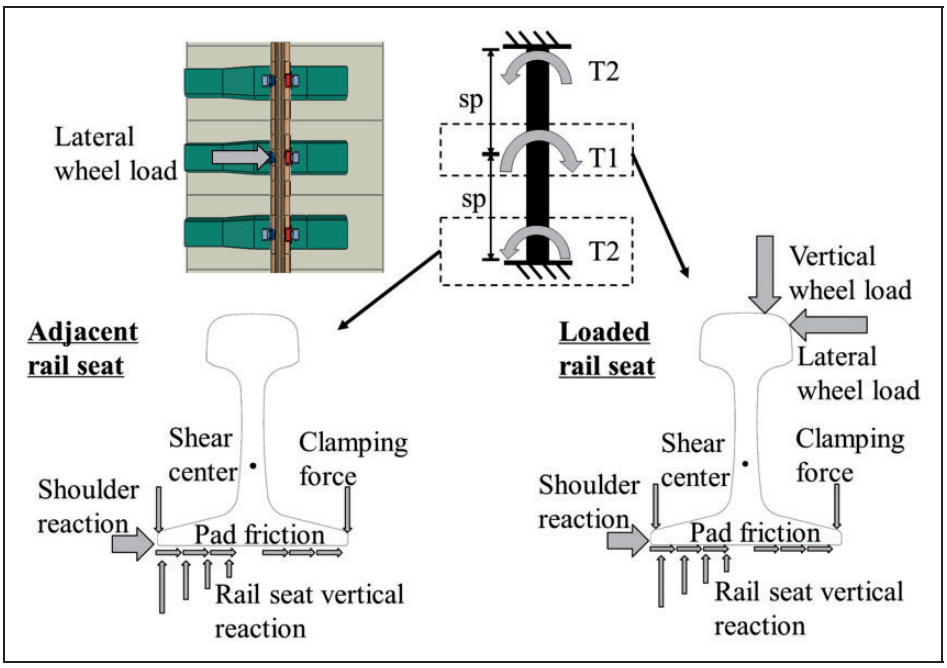

Figure 11. Framework of the mechanistic model for rail head rotational deflection.

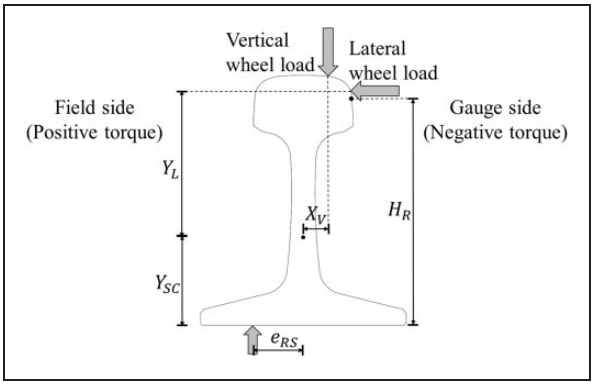

Figure 12. Dimensions of a rail section for torsion calculation.

gauge side, and the resultant torque should be negligible as the clamping forces are almost constant under minor rail deflection. However, the lever arm of the rail seat vertical reaction is affected by the wheel loading scenario and need to be specifically determined. Figure 12 shows dimensions of the rail section used in torsion calculation. As it is assumed that the rail only rotates between the two adjacent rail seats, based on torsional equilibrium there should be

$$\sum T_i = T_1 + 2T_2 = 0 \tag{11}$$

where T_1 and T_2 are the resultant torque due to wheel loads and rail seat reactions at the loaded rail seat and the adjacent rail seat (see Figure 11).

In the validated FE model, it is observed that the lever arm of the rail seat vertical reaction at the loaded rail seat is slightly larger than that at adjacent rail seats due to the rotation of the rail base. In the mechanistic model, it is assumed that the lever arms (e_{RS} in Figure 12) of the rail seat vertical reaction at different rail seats are the same, and based on the rail seat vertical and lateral reactions determined in the mechanistic model of RBLD, e_{RS} can be estimated with equation (11).

As in Figure 12, positive torque is defined as the torque that rotates the rail head to the field side. The resultant torque at the loaded and adjacent rail seats can be determined as

$$T_1 = LY_L + R_1 Y_{SC} - VX_V - V_1 e_{RS} \tag{12}$$

$$T_2 = R_2 Y_{SC} - V_2 e_{RS} \tag{13}$$

where X_V and Y_L are the lever arm of the vertical and lateral wheel load to the rail shear center, respectively; V_1 and V_2 are the rail seat vertical reaction at the loaded and adjacent rail seats, respectively; Y_{SC} is the height of shear center from the rail base; and V and L are the vertical and lateral wheel load, respectively. The rotation angle at the loaded rail seat can be determined as

$$\theta = \frac{T_2 sp}{J_R G_R} \tag{14}$$

where J_R and G_R are the torsional constant and shear modulus of the rail section, respectively. And the RHRD relative to the rail base at the loaded rail seat can be determined as

$$RHRD = H_R \sin\theta \approx H_R \theta \tag{15}$$

where H_R is the height from the rail base to the measurement point of the track gage. Combining the output of the two mechanistic models, the rail head lateral deflection can be estimated as the sum of the RBLD and the RHRD as

$$RHLD = RBLD + RHRD = \frac{(2R_2)(2sp)^3}{48E_R I_R} + \Delta_2 + H_R\theta \tag{16}$$

Validation of the mechanistic model

Comparison between the mechanistic model and the detailed FE model

It is important to validate the functionality of the mechanistic model on different designs of the fastening system and the track. To facilitate the future use of the developed mechanistic model as a potential design tool it was implemented in Microsoft Excel. The input and output parameters used in the implemented model are summarized in Table 2. Multiple graphic user forms were defined in the design tool for the design of different fastening system components, and the information are summarized later to predict the track response under a certain loading scenario.

Besides estimating the rail lateral deflection, the mechanistic model is also developed to better understand the lateral load path through the track structure. As laboratory or field measurement for the detailed behavior of fastening system components are not available, the prediction of the mechanistic model is compared with that of the validated FE model. As an example, in Figure 13 the behavior of the rail pad in the mechanistic model is compared with that in the FE model. The track configuration and loading scenario for this comparison are the same as in the field experimentation.[15] In the comparison, a two-stage linear behavior is observed in the prediction of the mechanistic model, as the closing of shoulder–insulator gap under increasing lateral wheel load changed the lateral stiffness of the loaded rail seat. Nonlinear behavior is observed in the FE model prediction due to the rotation of the rail. In general,

the prediction of the mechanistic model agrees with that of the FE model, which proves the mechanistic model is able to capture the lateral load path through the concrete crossties and the fastening systems.

In addition, the validated FE model is used to generate some cases and compared with the mechanistic model on rail head lateral deflection. The parameters and the corresponding ranges used in the experimental design are shown in Table 3. The ranges are determined based on the AREMA Manual and other references on engineering material properties.[2,18–21] A Latin hypercube sampling technique was used to select 120 representative configurations of the track structure from the design space, which ensures that the minimum distance between the sample points is maximized.[22] As the rail section is not a continuous variable, the rail sections used in the sample cases were lumped into three representative rail sections (100RE, 115RE, and 136RE).

In the mechanistic model, the rail head lateral deflection is divided into the RBLD and the RHRD, which are calculated separately. Therefore, it is reasonable to compare the two components between the mechanistic model and the FE model for any possible error. The comparison of the RBLD and the RHRD is shown in Figure 14. In both figures, the abscissa indicates the FE model prediction and the ordinate indicates the mechanistic model prediction. In the case of perfect agreement between both models, the sample points (points in diamond shape) should lie on the line with a slope of one (the black dash line in the figure).

In Figure 14(a), the sample points scatter closely to the dash line, which shows that the mechanistic model is capable of estimating the RBLD with minor error.

Table 2. Input and output of the mechanistic model.

Input	Output
Vertical wheel load	Rail head lateral deflection
Lateral wheel load	Rail base lateral deflection
Sleeper spacing	Rail head rotational deflection
rail section	
Insulator compression area	
Insulator compression thickness	
Insulator elastic modulus	
Shoulder elastic modulus	
Shoulder insert width	
Shoulder head height	
Shoulder insert length	
Shoulder insert height	
Shoulder–insulator gap size	
Rail pad elastic modulus	
Coefficient of friction	
Rail pad Poisson ratio	
Rail pad thickness	

Table 3. Parameters used in the experimental design for mechanistic model validation.

Input	Range
Sleeper spacing (m)	0.51–0.76
Rail section	100RE–136RE
Rail pad elastic modulus (MPa)	27.6–2758
Insulator elastic modulus (MPa)	2758–13790
Shoulder elastic modulus (MPa)	158,585–186,165
Vertical wheel load (kN)	26.7–177.9
L/V ratio	0–0.5
Rail seat coefficient of friction	0.12–1

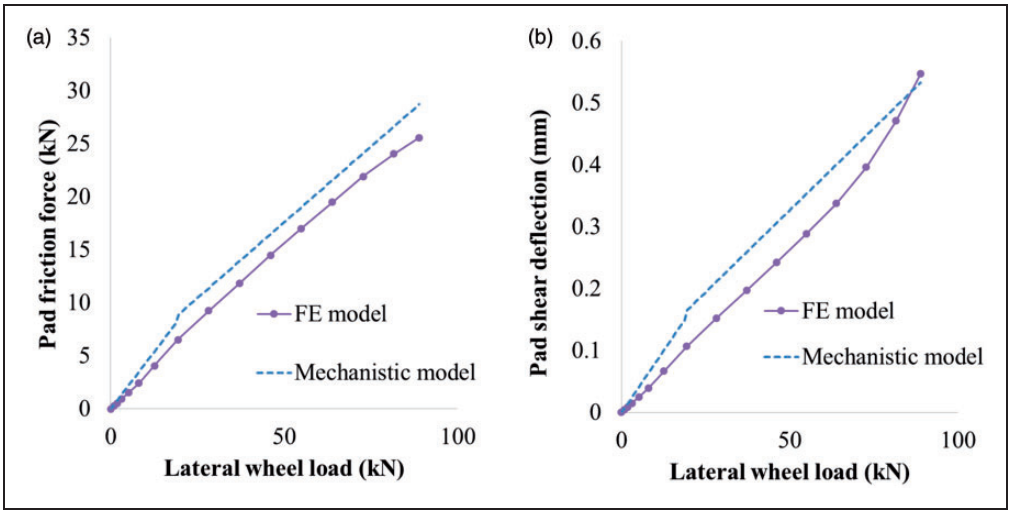

Figure 13. Comparison on (a) the pad friction force and (b) pad shear deflection between the FE model and the mechanistic model under field experimentation configuration (vertical wheel load = 178 kN (40 kips)).

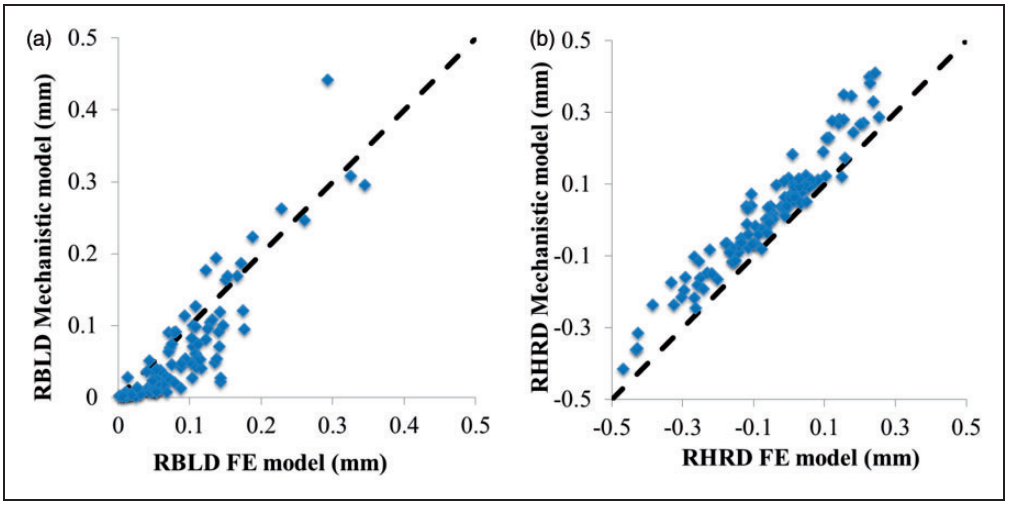

Figure 14. Comparison between (a) rail head lateral deflection (RBLD) and (b) rail head rotational deflection (RHRD) of the FE model and the mechanistic model.

The mechanistic model assumes linear behavior of the fastening system components, and as a result some nonlinear behaviors are not considered including the reduction of rail pad shear area due to rail base rotation and the yielding of fastening shoulders under larger lateral load. Considering the assumptions in the calculation of RBLD, it is reasonable that for a portion of the sample points the mechanistic model underestimate the RBLD when compared to the FE model.

In Figure 14(b), the distribution of the sample points is also quite close to the dash line. In addition, the error of the mechanistic model is relatively constant regardless of the prediction magnitude, which shows that the mechanistic model is able to capture the rotational mechanism of the rail. Under the torque of the vertical and lateral wheel load, the eccentricity of vertical rail seat reaction at the loaded rail seat should be larger than that at adjacent rail seats. As the mechanistic model assumes identical eccentricity of rail seat vertical reaction at different rail seats, it should overestimate the RHRD. However, as the mechanistic model only considers the torsional deflection of the rail with a length of twice the sleeper spacing rather than infinite length, the effect of the two assumptions offset to some extent. It can be observed that the effect of the mechanistic model assumptions agrees well with the comparison between the mechanistic model and the FE model.

Figure 15 shows the comparison between the rail head lateral deflection of the validated FE model and the mechanistic model. The diamond dots in the figure indicate the sample points included in the experimental design, and the dash line has a slope of one, which represents the case of perfect agreement. It can be observed that the prediction of the mechanistic model is quite close to that of the FE model.

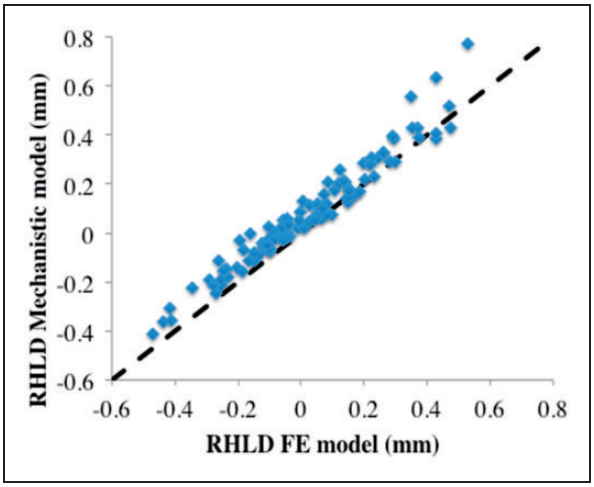

Figure 15. Comparison between the rail head lateral deflection (RHLD) of the FE model and the mechanistic model.

Comparison between the prediction of the mechanistic model and field measurement

As the mechanistic model is built considering some observations in the FE model, it should be compared with the field observations to ensure the assumptions of the mechanistic model are realistic. To investigate the wheel load path through the concrete sleeper and the fastening system, field experimentation was conducted at the Transportation Technology Center (TTC) at Pueblo, CO,[23] and the field measurement is used to validate the mechanistic model. As shown in Figure 16, in the static field experimentation 178 kN (40 kips) vertical wheel load and varying lateral wheel load (gauge-splitting load) was symmetrically applied to the two rail seats of a sleeper, and the same loading was repeated over each of the five instrumented crossties. At four of the rail seats, linear potentiometers

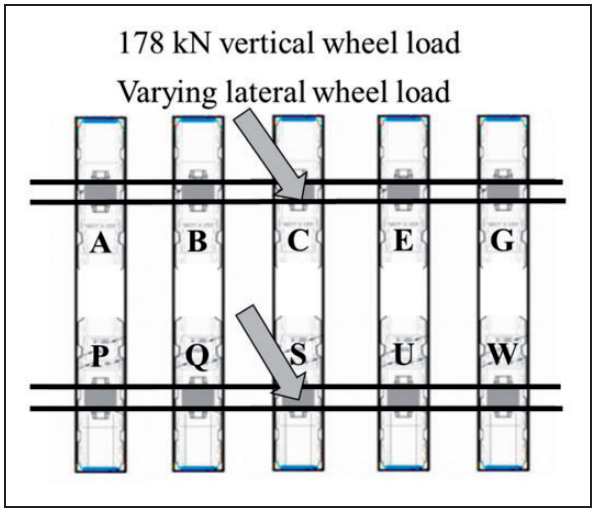

Figure 16. Naming of instrumented rail seats on instrumented track.

were installed to measure the lateral rail base and rail web lateral deflection under different loading scenarios, as shown in Figure 17.

As in the field experimentation, the rail lateral deflection was measured at the rail base and the rail web, the mechanistic model is modified to predict the rail web lateral deflection instead of the rail head lateral deflection. In the modified mechanistic model, the calculation of RBLD remains the same, while the distance H_R from the deflection measurement point to the rail base is reduced. The comparison on the rail web and RBLD between the field measurement, FE model, and the mechanistic model is shown in Figure 18(a) and (b), respectively. The deviation of the mechanistic model prediction at different loading levels is summarized in Table 4. While the response at different rail seats varies due to different support conditions and different gaps in the fastening system, the rail lateral deflection measured at the four

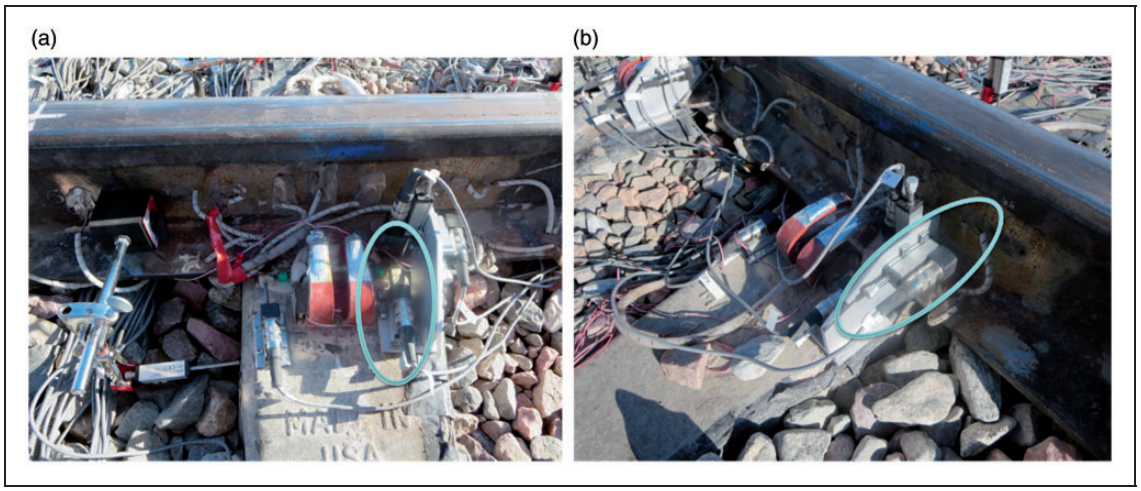

Figure 17. Linear potentiometers installed to measure (a) rail base lateral deflection and (b) rail web lateral deflection.

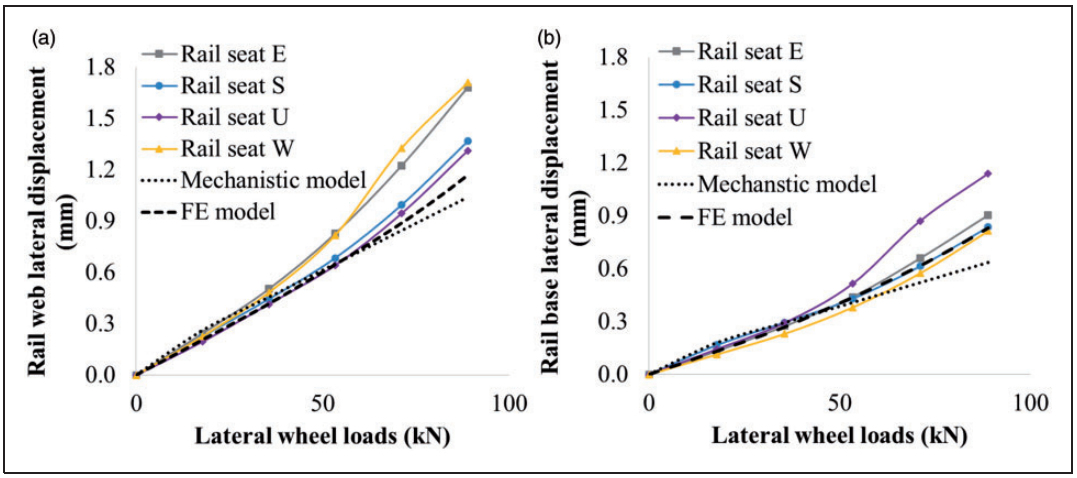

Figure 18. Comparison of (a) the rail web lateral deflection and (b) the rail base lateral deflection between the mechanistic model, FE model, and field track measurement (vertical wheel load = 178 kN (40 kips)).

Table 4. Summary of the field-measured rail lateral displacement and the corresponding deviation of the mechanistic model.

Lateral wheel load (kN)	Average rail base lateral displacement (mm)	Deviation of the mechanistic model (mm)	Average rail web lateral displacement (mm)	Deviation of the mechanistic model (mm)
0	0	0	0	0
17.79	0.140	–0.040	0.223	–0.038
35.58	0.274	–0.020	0.462	0.007
53.38	0.441	0.033	0.743	0.093
71.17	0.681	0.159	1.123	0.278
88.96	0.924	0.288	1.519	0.478

rail seats is quite close. In the field measurement, nonlinear behavior is observed as the track stiffness for rail lateral deflection (incremental lateral wheel load divided by incremental lateral deflection) decreased under higher lateral wheel load. The mechanistic model is able to capture the linear behavior of the track system under lower lateral wheel load, and slightly underestimate the rail lateral deflection under higher lateral wheel load due to linearity assumption.

The nonlinearity observed in the field measurement is mainly due to the rotation of the rail base. The area of rail pad effectively in shear will gradually reduce under larger rotation of the rail base, which results in reduced effective shear stiffness of the rail pad. However, in the current mechanistic model, the area of rail pad effectively in shear is assumed to be constant. As a result, the mechanistic model tends to slightly overestimate the lateral stiffness of the loaded rail seat k_1 under larger forces.

Conclusion

To quantify the distribution of the lateral wheel load through the track structure and introduce the mechanistic design methodology to the design of fastening system, a mechanistic model of rail head lateral deflection is developed in this study based on the design of the fastening system. With the use of track and fastening system input design parameters, the mechanistic model is able to calculate the corresponding rail head lateral deflection relative to the sleeper. The rail head lateral deflection is divided into the RBLD and the RHRD, and the two components are calculated separately. The developed mechanistic model was implemented in Microsoft Excel to facilitate its potential use as a design tool. Based on a design of experiment approach, the prediction of the mechanistic model is compared with the validated FE model to ensure its accuracy on fastening systems of different designs. In addition, to further validate the assumptions of the mechanistic model, it was also compared with field measurements from instrumented tracks in TTC at Pueblo, CO. Through this study, some conclusions related to the mechanistic model can be summarized:

1. Based on the comparison with the FE model, the mechanistic model could be used to estimate the rail lateral deflection in track structures of different designs.
2. Based on the comparison with field measurement, it is proven that the mechanistic model is able to capture the linear behavior of the track structure, and slightly underestimate the rail head lateral deflection under large lateral wheel load due to the nonlinearity of the fastening system.

The mechanistic model presented in this study is simplified as it only includes some track structure components (rail, shoulder, insulator, and rail pad, etc.) that are critical for the calculation of rail head lateral deflection. Considering the practical range of track design parameters, the contribution of these components should not be ignored. The error of the mechanistic model observed in the comparison with field measurement was due to the assumption of constant effective shear area of the rail pad. To incorporate the nonlinearity observed in field measurement, the proposed mechanistic model could be further improved by considering the effect of rail base rotation on the performance of the fastening system. Besides, the field experimentation and FE models are based on one design of prestressed concrete sleeper with a concrete compressive strength of 48.3 MPa (7000 psi), as this design of sleeper is widely installed on heavy-haul railroad in North America.[17] The developed model could also be improved by considering the effect of concrete strength on the interaction between the sleeper and the embedded shoulder.

Acknowledgement

The published material in this paper represents the position of the authors and not necessarily that of US DOT. Industry partnership and support has been provided by Union Pacific Railroad; BNSF Railway; National Railway Passenger Corporation (Amtrak); Amsted RPS; GIC;

Hanson Professional Services, Inc.; CXT Concrete Ties, Inc., an LB Foster Company; and TTX Company.

Declaration of Conflicting Interests

The author(s) declared no potential conflicts of interest with respect to the research, authorship, and/or publication of this article.

Funding

The author(s) disclosed receipt of the following financial support for the research, authorship, and/or publication of this article: The authors would like to express their sincere gratitude to the United States Department of Transportation (US DOT) FRA for providing funding for this research project.

References

1. Riessberger K. Treat them right and concrete sleepers will last half-a-century. *Railway Gazette Int* 1984; 140: 525–527.
2. AREMA. *Manual for railway engineering. Ties*. Lanham, MD: AREMA, 2012.
3. FRA. *Track safety standards class 6 through 9. Track and Rail and Infrastructure Integrity Compliance Manual*. Washington, DC: Federal Railroad Administration, 2012.
4. FRA. *International concrete crosstie and fastening system survey*. Washington, DC: Federal Railroad Administration, 2013.
5. Zarembski AM. Rail rollover—the state of the art. *AREA Bull* 1977, pp.12–20. AREA.
6. Marquis BP, Muhlanger M and Jeong DY. Effect of wheel/rail loads on concrete tie stresses and rail rollover. In: *ASME 2011 Rail Transportation Division Fall Technical Conference,* 2011, pp.143–150. New York, NY: American Society of Mechanical Engineers.
7. Wu H and Kerchof B. Management of wheel/rail interface to prevent rail rollover derailments. *Proc IMechE, Part F: J Rail and Rapid Transit*, Epub ahead of print 18 February 2014. DOI: 0954409714522222.
8. Choros J, Coltman MN and Marquis B. Prevention of derailments due to concrete tie rail seat deterioration. In: *ASME/IEEE 2007 Joint Rail Conference and Internal Combustion Engine Division Spring Technical Conference*, 2007, pp.173–181. New York, NY: American Society of Mechanical Engineers.
9. AREA. *Collected reports of the Special Committee on Stresses in Railroad Track*. S.l.1917.
10. Canadian National Railway. Wheel impact load detectors: the early history on CN. In: *Thirty-first Annual North American Rail Mechanical Operations Seminar*. St. Louis, Missouri: Association of American Railroads, 2011, pp.1–20.
11. Sato Y. On the lateral strength of railway track. *Railway Technical Research Institute, Quarterly Reports,* 1961, p.2. Kokubunji-shi, Tokyo: Railway technical research institute.
12. Timoshenko S and Langer B. Stresses in railroad track. In: *Proceedings of ASME*, 1973, pp.277–302. New York, NY.
13. Arbabi-Kanjoori F. Variational formulation of rail overturning and a finite element solution technique. In: *Proceedings of Fourth Annual Intersociety Conference on Transportation*, 1976. Warrendale, PA: Society of Automotive Engineers.
14. Turek J. Non-linear response of the track. *Vehicle Syst Dyn* 1995; 24: 265–279.
15. Williams BA, Kernes R, Edwards JR, et al. Lateral force measurement in concrete crosstie fastening systems. In: *Transportation Research Board 93rd Annual Meeting 2014 (No. 14-3112)*. Washington, DC.
16. Dassault Systemes Simulia Corp. *ABAQUS analysis user's manual, Version 6.11*. 2011.
17. Chen Z, Shin M, Wei S, et al. Finite element modeling and validation of the fastening systems and concrete sleepers used in North America. *Proc IMechE, Part F: J Rail and Rapid Transit*. Epub ahead of print 21 April 2014. DOI: 0954409714529558.
18. Harper CA. *Handbook of plastics, elastomers, and composites*. New York, NY: McGraw-Hill Inc., 1996.
19. Hepburn C. *Polyurethane elastomers*. London: Applied Science Publishers, 1982.
20. Stachowiak G and Batchelor AW. *Engineering tribology*. Atlanta, GA: Elsevier Science, 2013.
21. Yamaguchi Y. *Tribology of plastic materials: their characteristics and applications to sliding components*. Atlanta, GA: Elsevier Science, 1990.
22. McKay MD, Beckman RJ and Conover WJ. A comparison of three methods for selecting values of input variables in the analysis of output from a computer code. *Technometrics* 1979; 21: 239.
23. Grasse JS. *Field test program of the concrete crosstie and fastening system*. Urbana, IL: Department of Civil and Environmental Engineering, University of Illinois at Urbana-Champaign, 2013.

Appendix

Notation

A_{In}	contact area between the rail base and the insulator
A_{RP}	nominal contact area between the rail base and the rail pad
d_{In}	insulator thickness in compression
d_P	thickness of the rail pad
e_{RS}	lever arm of the rail seat vertical reaction to the rail shear center
E_{In}	elastic modulus of the insulator
E_R	elastic modulus of the rail
E_{SH}	elastic modulus of the shoulder
F_P	rail pad friction force
F_{PS}	the maximum rail pad frictional force based on the Coulomb Law
F_{SI}	shoulder bearing force
G_P	shear modulus of the rail pad
G_R	shear modulus of the rail
h_{SH}	height of the shoulder head
H_R	height from the rail base to the measurement point of the track gage
I_R	rail's moment of inertia about the vertical cross sectional axis
I_{SH}	area moment of inertia of the shoulder inserts
J_R	torsional constant of the rail section
k_1	lateral stiffness of the loaded rail seat

k_2	lateral stiffness of the adjacent rail seat
k_{insert}	stiffness of the shoulder insert
k_r	additional rotational stiffness at the top of shoulder insert
K_{In}	lateral stiffness of the insulator
K_P	shear stiffness of the rail pad
K_{SH}	lateral stiffness of the shoulder
K_{SI}	the resultant lateral stiffness of the insulator and the shoulder
l_{SH}	length of the shoulder insert
L	applied lateral wheel load
R_1	rail seat lateral load at the loaded rail seat
R_2	rail seat lateral load at the adjacent rail seat
sp	sleeper spacing
T_1	resultant torque at the loaded rail seat
T_2	resultant torque at the adjacent rail seat
V	vertical wheel load
V_1	rail seat vertical reaction at the loaded rail seat
V_2	rail seat vertical reaction at the adjacent rail seat
X_V	the lever arm of the vertical wheel load to the rail shear center
Y_L	the lever arm of the lateral wheel load to the rail shear center
Y_{SC}	height of the shear center from the rail base
$\boldsymbol{\delta}$	Size of the gap between the field-side shoulder and insulator
Δ_1	rail base lateral deflection at the loaded rail seat
Δ_2	rail base lateral deflection at the adjacent rail seat
Δ_I	top deflection of the shoulder insert
Δ_r	rotational deflection of the shoulder head
Δ_{SH}	deflection of the shoulder
θ	rotation angle of the rail at the loaded rail seat
θ_I	top rotation of the shoulder insert